Ultrafast Science
A SCIENCE PARTNER JOURNAL

RESEARCH ARTICLE

Subcycle Phase Matching Effects in Short Attosecond Pulse Trains

Nedjma Ouahioune[1*], Rodrigo Martin-Hernández[2,3], Dominik Hoff[1], Praveen Kumar Maroju[1], Chen Guo[1], Robin Weissenbilder[1], Sara Mikaelsson[1], Anne L'Huillier[1], Matteo Lucchini[4,5], Cord L. Arnold[1], and Mathieu Gisselbrecht[1*]

[1]Department of Physics, Lund University, Lund, Sweden. [2]Grupo de Investigación en Aplicaciones del Láser y Fotónica, Departamento de Fisica Aplicada, Universidad de Salamanca, Salamanca, Spain. [3]Unidad de Excelencia en Luz y Materia Estructuradas (LUMES), Universidad de Salamanca, Salamanca, Spain. [4]Department of Physics, Politecnico di Milano, 20133 Milan, Italy. [5]Institute for Photonics and Nanotechnologies, IFN-CNR, 20133 Milan, Italy.

*Address correspondence to: nedjma.ouahioune@fysik.lu.se (N.O.); mathieu.gisselbrecht@fysik.lu.se (M.G.)

Citation: Ouahioune N, Martin-Hernández R, Hoff D, Maroju PK, Guo C, Weissenbilder R, Mikaelsson S, L'Huillier A, Lucchini M, Arnold CL, et al. Subcycle Phase Matching Effects in Short Attosecond Pulse Trains. *Ultrafast Sci.* 2026;6:Article 0154. https://doi.org/10.34133/ultrafastscience.0154

Submitted 5 December 2025
Revised 16 February 2026
Accepted 4 March 2026
Published 7 May 2026

Attosecond pulses produced by high-order harmonic generation in gases driven by intense laser fields have become a cornerstone technique for probing ultrafast electronic motion in matter. These applications require a good knowledge of the temporal and spectral properties of the emitted radiation. In this work, we generate a train of 2 to 3 attosecond pulses that we characterize using 2-color laser-assisted photoionization. An unexpected spectral behavior, with more pulses at high energies than at low energies, is observed when the carrier-to-envelope phase of the laser field is changed by 90°. High-order harmonic generation simulations indicate that the time-dependent phase matching of the harmonics contributes in a nontrivial way to the structure of the pulse train. Two-color laser-assisted photoionization enables us to unravel the dynamical influence of subcycle phase matching on the spectral properties of the attosecond pulse train, going beyond the predictions of the response of a single atom to a strong laser field.

Introduction

The generation of high-order harmonics of an intense laser in gas targets [1,2] has enabled the production of attosecond pulses of light in the extreme-ultraviolet (XUV) range [3,4]. The process depends on the highly nonlinear interaction of the intense laser with an isolated atom (or a molecule)—a microscopic effect known as the single-atom response [5–7]—and the in-phase propagation of the generated XUV radiation and the driving laser field—a macroscopic effect called phase matching [8–10]. In general, the properties of the attosecond pulses depend on the interplay between the single-atom response and propagation effects, which influences the efficiency, coherence, and spatio-temporal structure of the XUV emission [11–14]. The impact of the reshaping of the fundamental field on high-order harmonic generation (HHG) has also been pointed out for high laser intensities [15–19].

The generation of high-order harmonics is due to the interference of attosecond pulses (temporal slits) created in the subcycle light–matter interaction [20], similar to the emission of electrons in above-threshold ionization (ATI), due to the interference of attosecond electron wave packets [21]. In HHG, the harmonics are separated by twice the laser photon energy, while in ATI, the detection breaks the inversion symmetry, and electron energy peaks are separated by the laser photon energy. When the laser pulse is short (≤10 fs), the number of slits is small and the spectral range of the attosecond pulses differ from one half-cycle to the next. In the single-atom response, this spectral range can be obtained simply from the cutoff law [7,22], as shown schematically in Fig. 1.

Attosecond pulses can be temporally characterized using laser-assisted photoionization schemes such as streaking [4,13,23] and RABBIT (reconstruction of attosecond beating by interference of 2-photon transitions) [3,24]. In these schemes, electron spectra are measured as a function of the delay between the XUV radiation and a phase-locked infrared (IR) field. In streaking, the electron energy oscillates and the temporal properties can be obtained from the amplitude and contrast of these oscillations [25]. In RABBIT, the absorption/emission of an additional IR photon leads to additional peaks, called sidebands, and the temporal properties of an average attosecond pulse in a train can be obtained from the phase of the sideband oscillations [3,26]. In both cases, retrieval methods taking advantage of the entire spectrum as a function of delay have been successfully developed [25–31].

In this work, we create attosecond pulse trains (APTs) using few-cycle laser pulses, with a stable carrier-to-envelope phase (CEP), focused in a gas of argon atoms. Due to the short laser duration (≤6 fs), the APTs contain a few attosecond pulses [20] and their number depends on the CEP of the driving laser. We characterize these APTs by laser-assisted photoionization of helium using a 3-dimensional momentum spectrometer [32]. For certain CEP values, the spectrograms, which are the

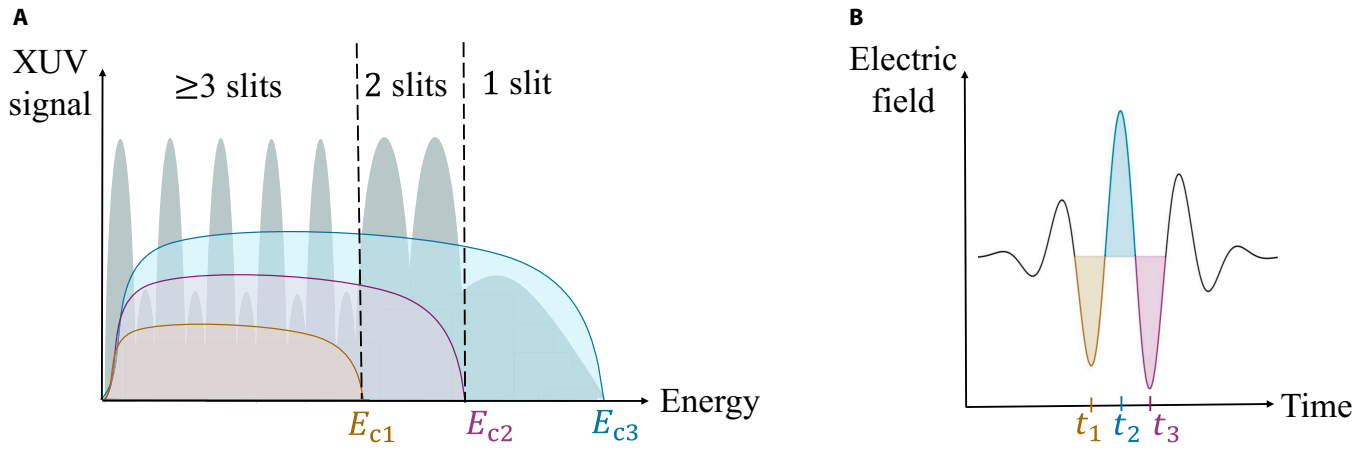

Fig. 1. (A) Illustration of the spectral content of attosecond pulses (temporal slits) generated in each half-cycle of a short laser pulse, shown in (B). Each color (purple, blue, and orange) refers to a specific pulse, with a unique cutoff energy E_c. The pattern resulting from the interference is shown in gray.

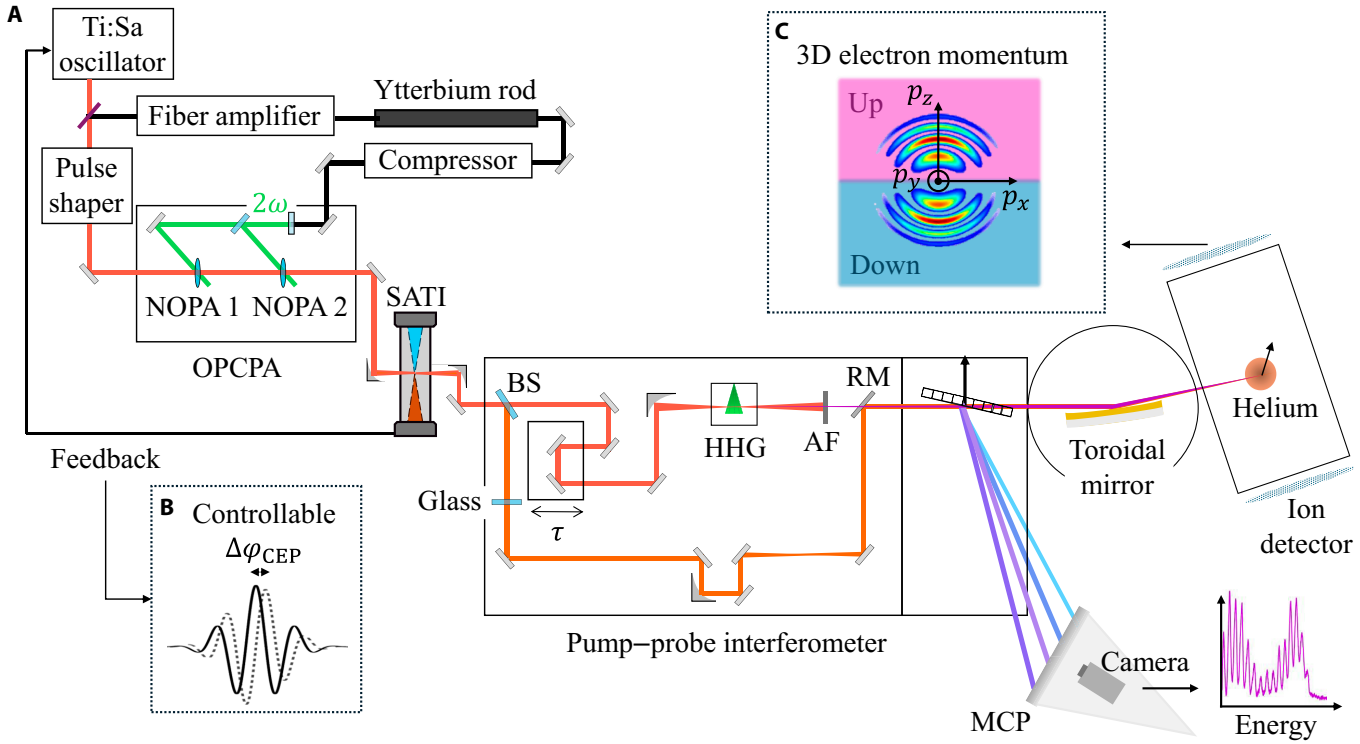

Fig. 2. (A) Schematic of the experimental setup. Laser pulses from a Ti:sapphire oscillator are amplified using 2 nonlinear optical parametric amplification (NOPA) stages. The relative carrier-to-envelope phase (CEP) of the output pulses is controlled shot to shot through the feedback of a stereo above-threshold-ionization (SATI) device to a wedge pair in the oscillator [33]. The CEP-controlled pulses are separated into a probe arm and a variably delayed pump arm by a beam splitter (BS). Short attosecond pulse trains are produced by the infrared (IR) driving field using high-order harmonic generation (HHG) and recombined with the probe before being focused into the sensitive region of a 3-dimensional electron spectrometer. (B) The controllable relative CEP $\Delta\varphi_{CEP}$ of the ≲6-fs laser pulses. (C) Momentum projected along p_x and p_z of the photoemitted electrons. The electrons can be distinguished between those emitted with $p_z > 0$ ("up") and those emitted with $p_z < 0$ ("down"), where z is the axis along the detector and of the polarization of the light. AF, aluminum filter; RM, recombination mirror; MCP, microchannel plate.

electron energy spectra as a function of delay, exhibit features that cannot be explained by the structure of the APTs predicted by the single-atom response alone. This is confirmed by a time–frequency analysis of the APTs retrieved from the experimental data [27,30]. Supported by 3-dimensional simulations and a 1-dimensional model, we show that the temporal properties of the APTs are also influenced by time-dependent phase matching in the nonlinear medium, with, in some cases, a non-trivial number of pulses as a function of the XUV energy. This experimental and theoretical study emphasizes the importance of subcycle phase matching for the accurate prediction and manipulation of the properties of attosecond light pulses.

Methods

The experiment, shown in Fig. 2, was performed using an optical parametric chirped pulse amplification system, providing sub-6-fs-long pulses at a central wavelength of 850 nm with up

to 10-μm pulse energy at a repetition rate of 200 kHz [32]. A stereo-ATI setup installed in the beam path stabilized the CEP on a shot-to-shot basis, providing stability of around 160 mrad (corresponding to a precision of 10°) [33]. Furthermore, the CEP was controlled by a wedge pair in the oscillator (not shown in the schematic). The laser beam was then split into a pump (XUV) and a probe (IR) arm by a beam splitter. In the pump arm, the beam was tightly focused (beam waist $w_0 = 5$ μm and Rayleigh length $z_R \sim 100$ μm) into a thin argon gas jet (~36-μm length) at a pressure of 4 bar, reaching an intensity of ~1.5×10^{14} W/cm^2 to generate a comb of phase-locked odd-order harmonics. The low-order harmonics, below ~15 eV, and the generating field were filtered out with an aluminum foil of 200 nm. The XUV pump was recombined with the probe using a holey mirror (recombination mirror). The delay τ between the XUV and the IR in the probe arm could be controlled using a delay stage in the pump arm. Once recombined, both fields were focused by a toroidal mirror into a helium gas target; the probe intensity was estimated to be ~10^{11} W/cm^2. A reaction microscope was used to measure the 3-dimensional momentum of the photoelectrons created by the absorption of the XUV-only or the XUV + IR radiation. In our experiments, the delay between the XUV light and the IR probe was scanned for different CEP settings. Changing the CEP allowed us to vary the number of pulses in the train, typically between 2 and 4 [20].

Results and Discussion

Figure 3A and C presents photoelectron spectra as a function of the delay for 2 different CEP values separated by 90°. In the figure, only electrons emitted in a solid angle of $+2\pi$ sr ("up") along the common polarization axis of XUV and IR fields are shown (see Fig. 2) [20]. At large delays, when the fields do not overlap, the photoelectron peaks are separated by a kinetic energy of $2\hbar\omega$ ($\hbar$ is the reduced Planck constant, and ω is the laser frequency) due to single-photon ionization by the comb of harmonics. At delays where the XUV and the IR overlap, additional features form, which depend on the kinetic energy and the CEP. Above 10 eV in Fig. 3A and between 7 and 10 eV in Fig. 3C, the kinetic energy of the photoelectrons oscillates as a function of the delay with a periodicity equal to the laser period ~2.6 fs. In other spectral regions, additional electron peaks are observed at kinetic energies between those due to the absorption of consecutive harmonics. In particular, in Fig. 3C, the pattern looks like a "chessboard" over a large energy range from 12 eV to the highest observed energy. This remarkable energy dependence comes from the small number of attosecond pulses in the train. Oscillations arise from the interference between 2 electron wave packets, similar to a double-slit experiment [20]. The additional electron peaks are due to the interference of more than 2 electron wave packets, leading to sidebands, similar to RABBIT measurements performed with multiple-cycle pulses [3,24].

In the Supplementary Materials, we also show the spectra obtained by collecting electrons emitted in the opposite direction ("down") in Fig. S1. The results are very similar to Fig. 3A and C, except that the positions of the maxima and minima of the oscillations are shifted by half a laser period [20]. Consequently, collecting electrons over the full solid angle removes the CEP-dependent features. We note that the behavior of the photoelectron spectra does not vary much with angle in each hemisphere.

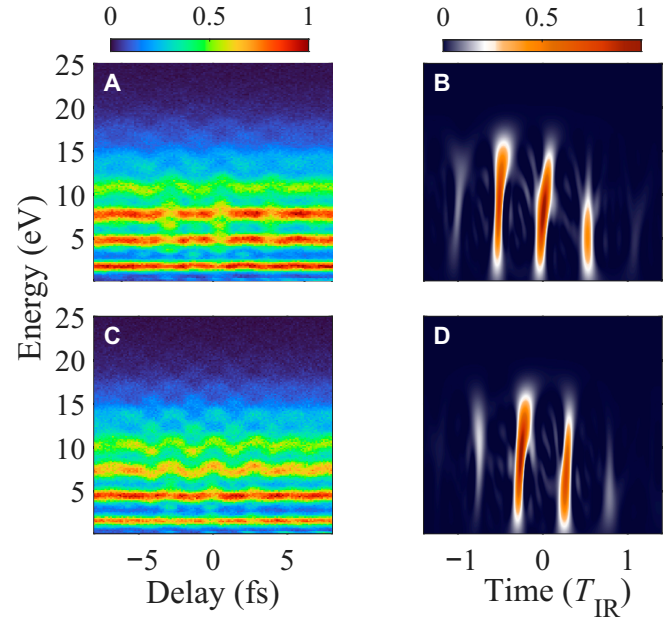

Fig. 3. (A and C) Experimental photoelectron spectra as a function of the extreme ultraviolet (XUV)–infrared (IR) delay for 2 different carrier-to-envelope phase (CEP) values separated by 90°. Only electrons photoemitted in the upper hemisphere around the polarization axis of the light fields are shown. (B and D) Wigner distributions of the attosecond pulses retrieved from the experimental spectrograms through the refined extended ptychographic iterative engine (rePIE) [28].

In the single-atom response, illustrated in Fig. 1, the minimum driving field intensity $I_{\min}(q)$ required for a harmonic order q to reach the plateau region can be obtained from the cutoff law, $q\hbar\omega = I_p + 3.17U_p$, where I_p is the ionization energy of argon and U_p is the ponderomotive energy equal to $\alpha hI/(m_e\omega^2)$. In this expression, α is the fine structure constant, I is the laser intensity, and m_e is the electron mass. This intensity, expressed as

$$I_{\min}(q) = \frac{m_e\omega^2}{3.17\alpha h}\left(q\hbar\omega - I_p\right), \quad (1)$$

increases linearly as a function of the harmonic order q. For our few-cycle pulses (≤6 fs), this implies that the highest-order harmonics are generated only during a few half-cycles of the electric field at the center of the pulse. Consequently, the number of attosecond pulses in the train depends on a chosen spectral range. It decreases as the central photon energy increases. With our ultrashort pulses, only 2 half-cycles (or less) reach the intensity for the generation of the highest orders. On the other hand, lower-order harmonics are generated over many half-cycles. The above argument would always result in RABBIT-like features at low photoelectron kinetic energies and an oscillatory pattern (streaking-like pattern) at higher photoelectron energies, for any CEP. From these arguments, the experimental observation in Fig. 3C cannot be explained.

To understand the temporal structure of the APTs, we apply the refined extended ptychographic iterative engine [27,28,30], described in the Supplementary Materials. The retrieved spectrograms are in good agreement with the experimental ones, as shown in Fig. S2 of the Supplementary Materials. We describe the properties of the APTs using the Wigner distribution, defined as

$$W(t,\Omega) = \int_{-\infty}^{+\infty} \mathcal{E}_{\mathrm{APT}}\left(t+\frac{\tau}{2}\right)\mathcal{E}^*_{\mathrm{APT}}\left(t-\frac{\tau}{2}\right)e^{-i\Omega\tau}\,d\tau, \quad (2)$$

where Ω is the XUV frequency and $\mathcal{E}_{\mathrm{APT}}$ is the XUV field. The advantage of using the Wigner distribution compared to other time–frequency representations is that the spectral and temporal resolution is limited only by the uncertainty principle. Figure 3B and D shows the Wigner representations for the APTs retrieved from the experimental results in Fig. 3A and C. Figure 3B shows essentially 3 pulses at low energies and 2 pulses above 12 eV. In comparison, Fig. 3D shows 2 dominating pulses up to 10 eV and 3 pulses at higher energies. The observed spectral variation of the structure of the APT cannot be explained by considering only the single-atom response.

We performed advanced HHG simulations that account for both microscopic and macroscopic effects. Specifically, we compute the far-field harmonic emission by solving the Schrödinger equation within the strong field approximation (SFA) [6] and by including the propagation and absorption of the fundamental and harmonic fields in a thin nonlinear medium while accounting for the longitudinal phase matching of the XUV radiation [34]. This calculation goes beyond the slowly varying envelope approximation, including in particular subcycle ionization dynamics with the Yudin–Ivanov CEP-dependent model described in Ref. [35]. The driving laser field is defined as $E(t) = E_0 f(t)\exp\left[i\left(\omega t + \varphi_{\mathrm{CEP}}\right)\right]$ where E_0 is the amplitude of the electric field, $f(t) = \sin^2\left(\pi t/t_{\mathrm{p}}\right)$ (for $0 \le t \le t_{\mathrm{p}}$), and φ_{CEP} is the CEP. We perform a systematic study of HHG as a function of pressure, intensity, pulse duration, and focusing conditions. We find that our observations are well reproduced for the parameters corresponding to the experimental ones (see the methods section). An exception is the pulse duration, which is chosen to be 4.85 fs, slightly less than the experimental estimation (~6 fs). In these conditions, the ionization degree is relatively small, typically a few percent. Ground-state depletion is negligible, and the driving laser is not substantially reshaped during propagation. The single-atom response can be considered to be uniform throughout propagation in the gas; see Section 5.3 of the Supplementary Materials. The calculated APTs are then used to simulate laser-assisted photoionization spectra using SFA. The results shown in Fig. 4A and C, using CEPs of 70° and 160°, reproduce the experimental trends. The Wigner representations in Fig. 4B and D are similar to those obtained from the retrieved APTs (see Fig. 3), showing the same number of pulses across the different energy regions and an overall good agreement with the experiment. A noticeable difference is the tilt observed in the simulation due to the attosecond chirp [24]. The absence of tilt in the experiment likely originates from the aluminum filter, which compensates for the attosecond chirp [26]. The effect of the spectral phase variation due to photoionization is here negligible. These theoretical results confirm that CEP-dependent macroscopic effects influence in a nontrivial way the spectral content of the individual attosecond pulses.

To gain insight into the influence of macroscopic effects on the pulse train, we developed a one-dimensional model of time-dependent harmonic phase matching, including subcycle variations. The total phase mismatch $\Delta k(q,t)$ depends on the medium properties and on the laser parameters and can be written as [10]

$$\Delta k(q,t) = \Delta k_{\mathrm{foc}}(q) + \Delta k_{\mathrm{at}}(q) + \Delta k_{\mathrm{dip}}(q,t) + \Delta k_{\mathrm{fe}}(q,t), \quad (3)$$

where $\Delta k_{\mathrm{foc}}(q) = -q/z_{\mathrm{r}}$ comes from the laser focusing (through the variation of the Gouy phase over the Rayleigh length z_{r}), $\Delta k_{\mathrm{at}}(q)$ is due to the dispersion of the neutral

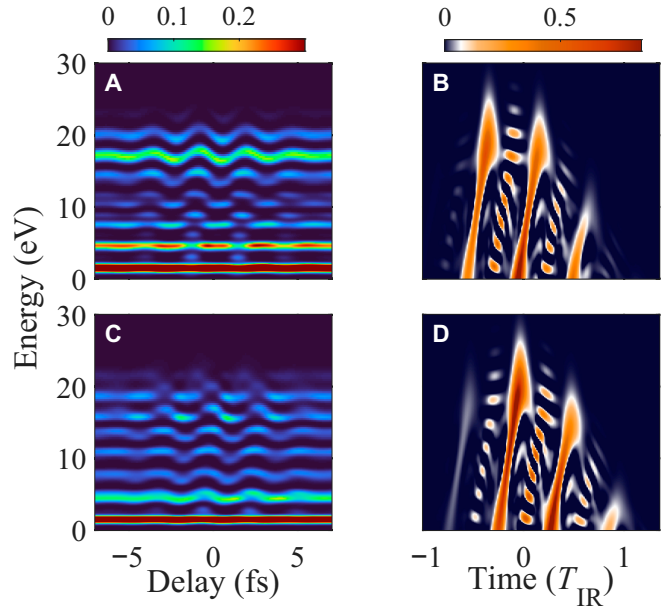

Fig. 4. (A and C) Photoionization spectrograms as a function of the kinetic energy of the electrons and of the extreme ultraviolet (XUV)–infrared (IR) delay simulated using the 3-dimensional model. (B and D) Wigner representation of the simulated attosecond pulse trains. The carrier-to-envelope phases (CEPs) are (A and B) 70° and (C and D) 160°.

medium, $\Delta k_{\mathrm{dip}}(q,t)$ comes from the dipole phase with the time-dependent intensity taking into account only the short trajectory contribution, and $\Delta k_{\mathrm{fe}}(q,t) \propto -q\rho\eta_{\mathrm{fe}}(t)$ is due to the free electrons and depends on the time-dependent ionization degree $\eta_{\mathrm{fe}}(t)$. The ionization degree is often estimated using a cycle-averaged approximation [10,36,37]. Here, we account for the subcycle variation of the ionization degree, allowing us to include CEP effects. In addition, we neglect the CEP slip across the focus as the medium length is small compared to the Rayleigh length.

Figure 5A and C shows the temporal variation of $\Delta k(q,t)$ for 5 harmonic orders and 2 CEPs equal to 70° and 160°. $\Delta k(q,t)$ strongly varies with time and for the different orders. The steps reflect the variation of $\Delta k_{\mathrm{fe}}(q,t)$ through the ionization rate. The difference in heights between the curves comes from the q dependence of the atomic dispersion $\Delta k_{\mathrm{at}}(q)$ and the dipole phase $\Delta k_{\mathrm{dip}}(q,t)$. Perfect phase matching ($\Delta k = 0$) is in general achieved only during a short time, less than one laser period, leading to temporal confinement of the harmonic emission. This time interval, in the conditions examined in the present work, moves to a later time as the harmonic order increases. At a CEP of 70°, phase matching, corresponding to $\left|\Delta k(q,t)\right| \le 0.03\ \ \mu\mathrm{m}^{-1}$, is achieved simultaneously for all harmonics. At a CEP of 160°, it is achieved at a later time and differently for harmonics 17 to 21 and harmonics 23 to 25.

For on-axis propagation in a uniform gas density, the intensity of the qth harmonic field at the exit of the medium can be expressed as [38,39]

$$I(q,t) \propto \left[\rho d(q,t)\right]^2 \frac{\cosh\left[\kappa_q L\right] - \cos\left[\Delta k(q,t) L\right]}{\kappa_q^2 + \Delta k^2(q,t)} e^{-\kappa_q L}, \quad (4)$$

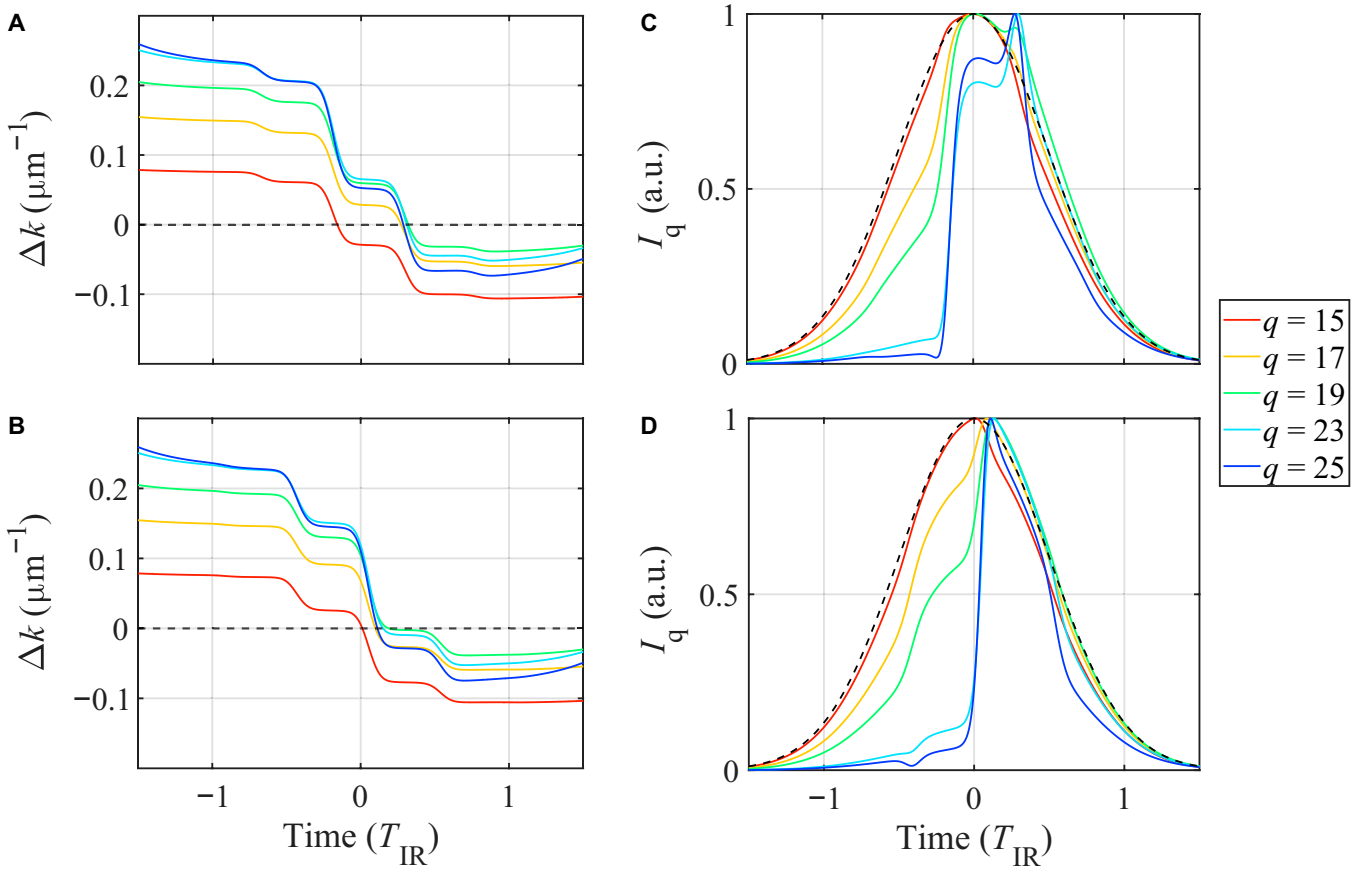

Fig. 5. (A and B) Total phase mismatch as a function of time in units of the laser period (T_{IR}) for 4 harmonic orders q for the carrier-to-envelope phases (CEPs) corresponding to Fig. 3B. The horizontal black dashed line corresponds to perfect phase matching. (C and D) Corresponding yield for each harmonic order q. The CEPs are 70° (top) and 160° (bottom). Dashed lines indicate the temporal profile of the single-atom response.

where $d(q, t)$ is the dipole moment obtained by using an effective power law dependence ($|d|^2 \propto I^{2.6}$) [10], $\rho = 8.8\ \mathrm{kg/m^3}$ is the experimental gas density, $L = 36$ μm is the medium length, and κ_q is the absorption coefficient [40]. The laser spatiotemporal properties are assumed constant throughout the interaction length since reshaping effects were found negligible (see the Supplementary Materials). The spectrograms simulated using this model, shown in Fig. S4 of the Supplementary Materials, reproduce the experimental observations, in contrast to those obtained with the single-atom response (see Fig. S5).

Figure 5B and D presents the harmonic intensity as a function of time for different harmonic orders and CEPs equal to 70° and 160°. In this model, the single-atom response leads to a temporal dependence $\propto I^{2.6}(t)$ for all harmonics, shown in dashed lines, while the inclusion of phase matching adds a subcycle q-dependent modulation of the temporal profile following the variation of $\Delta k(q,t)$ (see Fig. 5A and C). We observe that phase matching leads to a temporal confinement of the high-order harmonics. At a CEP of 160°, harmonics 23 and 25 are generated after the maximum intensity of the driving pulse and temporally confined to less than a half-cycle. In contrast, at 70°, all harmonics appear before the maximum intensity and are generated over a longer time. CEP-dependent phase matching changes the relative strength and duration of the attosecond pulses, depending on the spectral region, as observed in our experimental and theoretical results (see Figs. 3 and 4). In XUV far-field spectra, variations in the number of slits can be observed with pressure, as shown in Fig. S6 of the Supplementary Materials. While this model provides a valuable insight into the influence of phase matching on the spectro-temporal structure of the attosecond pulses, it cannot describe the details of the complex 3-dimensional spatiotemporal dynamics of the generation process.

Conclusion

In conclusion, we show that photoionization by short APTs in the presence of a dressing field leads to CEP-dependent photoelectron spectra. Our study emphasizes the sensitivity of laser-assisted photoionization for retrieving the intricate time–frequency dependence of short APTs. The behavior of photoelectron spectra can be explained by subcycle phase matching, which leads to temporal confinement of some harmonics, thereby acting as a passive pulse shaper. The spectral amplitude of each attosecond pulse in the train, therefore, varies in a nontrivial way, depending on the CEP. This work provides a comprehensive experimental and theoretical insight into subcycle phase-matching dynamics for short APTs.

Acknowledgments

We thank E. Constant for fruitful discussions.
Funding: M.G., A.L., and C.L.A. acknowledge support from the Swedish Research Council (Grant Nos. 2020-05200, 2023-04603, and 2021-04691) and the Knut and Alice Wallenberg

Foundation. A.L. acknowledges support from the European Research Council (Grant Nos. 884900 and 851201) and the Knut and Alice Wallenberg Foundation through the Wallenberg Centre for Quantum Technology (WACQT). This project has also received funding from the Ministerio de Ciencia e Innovación (grant PID2022-142340NB-I00) and from the Department of Education of the Junta de Castilla y León and FEDER Funds (Escalera de Excelencia CLU-2023-1-02 and Grant No. SA108P24).

Author contributions: N.O. analyzed the data and conceived the 1-dimensional model. R.M.-H. performed the 3-dimensional simulation. D.H. and S.M. performed the experiments. N.O. performed additional experiments. P.K.M. performed complementary analysis. C.G., C.L.A., and S.M. designed and constructed the light sources. M.L. performed the retrieval of the experimental data. P.K.M., R.W., C.L.A., C.G., A.L., and M.G. contributed to the scientific discussion. M.G. supervised the work. N.O. wrote the manuscript with inputs from A.L. and M.G. All authors provided feedback on the manuscript.

Competing interests: The authors declare that they have no competing interests.

Data Availability

Data underlying the results presented in this paper are not publicly available at this time but may be obtained from the authors upon reasonable request.

Supplementary Materials

Supplementary Text
Figs. S1 to S6
Reference [41]

References

1. Ferray M, L'Huillier A, Li X, Lompre L, Mainfray G, Manus C. Multiple-harmonic con version of 1064 nm radiation in rare gases. *J Phys B Atom Molec Opt Phys*. 1988;21(3):L31–L35.
2. McPherson A, Gibson G, Jara H, Johann U, Luk TS, McIntyre IA, Boyer K, Rhodes CK. Studies of multiphoton production of vacuum-ultraviolet radiation in the rare gases. *J Opt Soc Am B*. 1987;4(4):595–601.
3. Paul PM, Toma ES, Breger P, Mullot G, Augé F, Balcou P, Muller HG, Agostini P. Observation of a train of attosecond pulses from high harmonic generation. *Science*. 2001;292(5522):1689–1692.
4. Hentschel M, Kienberger R, Spielmann C, Reider GA, Milosevic N, Brabec T, Corkum P, Heinzmann U, Drescher M, Krausz F. Attosecond metrology. *Nature*. 2001;414:509–513.
5. Kulander KC, Schafer KJ, Krause JL. Dynamics of short-pulse excitation, ionization and harmonic conversion. In: Piraux B, L'Huillier A, Rzążewski K, editors. *Super-intense laser—Atom physics*. Boston (MA): Springer; 1993. p. 95–110.
6. Lewenstein M, Balcou P, Ivanov MY, L'Huillier A, Corkum PB. Theory of high-harmonic generation by low-frequency laser fields. *Phys Rev A*. 1994;49(3):2117–2132.
7. Corkum PB. Plasma perspective on strong field multiphoton ionization. *Phys Rev Lett*. 1993;71(13):1994–1997.
8. L'Huillier A, Balcou P, Candel S, Schafer K, Kulander K. Calculations of high-order harmonic-generation processes in xenon at 1064 nm. *Phys Rev A*. 1992;46(5):2778–2790.
9. Balcou P, Salières P, L'Huillier A, Lewenstein M. Generalized phase-matching conditions for high harmonics: The role of field-gradient forces. *Phys Rev A*. 1997;55(4):3204–3210.
10. Weissenbilder R, Carlström S, Rego L, Guo C, Heyl CM, Smorenburg P, Constant E, Arnold CL, L'Huillier A. How to optimize high-order harmonic generation in gases. *Nat Rev Phys*. 2022;4(11):713–722.
11. Kazamias S, Douillet D, Weihe F, Valentin C, Rousse A, Sebban S, Grillon G, Augé F, Hulin D, Balcou P, et al. Global optimization of high harmonic generation. *Phys Rev Lett*. 2003;90(19):Article 193901.
12. Ferrari F, Calegari F, Lucchini M, Vozzi C, Stagira S, Sansone G, Nisoli M. High-energy isolated attosecond pulses generated by above-saturation few-cycle fields. *Nat Photonics*. 2010;4(12):875–879.
13. Sansone G, Benedetti E, Calegari F, Vozzi C, Avaldi L, Flammini R, Poletto L, Villoresi P, Altucci C, Velotta R, et al. Isolated single-cycle attosecond pulses. *Science*. 2006;314(5798):443–446.
14. Wikmark H, Guo C, Vogelsang J, Smorenburg PW, Coudert-Alteirac H, Lahl J, Peschel J, Rudawski P, Dacasa H, Carlström S, et al. Spatiotemporal coupling of attosecond pulses. *Proc Natl Acad Sci*. 2019;116:4779–4787.
15. Gaarde MB, Schafer KJ. Generating single attosecond pulses via spatial filtering. *Opt Lett*. 2006;31(21):3188–3190.
16. Major B, Kretschmar M, Ghafur O, Hoffmann A, Kovács K, Varjú K, Senfftleben B, Tümmler J, Will I, Nagy T, et al. Propagation-assisted generation of intense few femtosecond high-harmonic pulses. *J Phys Photonics*. 2020;2(3):Article 034002.
17. Major B, Kovács K, Svirplys E, Anus M, Ghafur O, Varjú K, Vrakking MJJ, Tosa V, Schütte B. A compact, easily tunable extreme-ultraviolet source: High-harmonic generation in strongly overdriven regime. Paper presented at: Frontiers in Optics + Laser Science 2024 (FiO, LS); 2024 Sep 23–26; Denver, CO.
18. Kretschmar M, Svirplys E, Volkov M, Witting T, Nagy T, Vrakking MJJ, Schütte B. Compact realization of all-attosecond pump-probe spectroscopy. *Sci Adv*. 2024;10(8):eadk9605.
19. Vismarra F, Fernández-Galán M, Mocci D, Colaizzi L, Segundo VW, Boyero-García R, Serrano J, Conejero-Jarque E, Pini M, Mai L, et al. Isolated attosecond pulse generation in a semi-infinite gas cell driven by time-gated phase matching. *Light Sci Appl*. 2024;13(1):197.
20. Cheng YC, Mikaelsson S, Nandi S, Rämisch L, Guo C, Carlström S, Harth A, Vogelsang J, Miranda M, Arnold CL, et al. Controlling photoionization using attosecond time-slit interferences. *PNAS*. 2020;117(20):10727–10732.
21. Lindner F, Schätzel MG, Walther H, Baltuska A, Goulielmakis E, Krausz F, Milosević DB, Bauer D, Becker W, Paulus GG. Attosecond double-slit experiment. *Phys Rev Lett*. 2005;95(4):Article 040401.
22. Krause JL, Schafer KJ, Kulander KC. High-order harmonic generation from atoms and ions in the high intensity regime. *Phys Rev Lett*. 1992;68(24):3535–3538.
23. Goulielmakis E, Schultze M, Hofstetter M, Yakovlev VS, Gagnon J, Uiberacker M, Aquila AL, Gullikson EM, Attwood DT, Kienberger P, et al. Single-cycle nonlinear optics. *Science*. 2008;320(5883):1614–1617.
24. Mairesse Y, de Bohan A, Frasinski L, Merdji H, Dinu LC, Monchicourt P, Breger P, Kovacev M, Taïeb R, Carré B, et al.

Attosecond synchronization of high-harmonic soft x-rays. *Science*. 2003;302(5650):1540–1543.
25. Mairesse Y, Quéré F. Frequency-resolved optical gating for complete reconstruction of attosecond bursts. *Phys Rev A*. 2005;71(1):Article 011401.
26. Lopez-Martens R, Varjú K, Johnsson P, Mauritsson J, Mairesse Y, Salières P, Gaarde MB, Schafer KJ, Persson A, Svanberg S, et al. Amplitude and phase control of attosecond light pulses. *Phys Rev Lett*. 2005;94(3):Article 033001.
27. Lucchini M, Lucchini M, Brügmann MH, Ludwig A, Gallmann L, Keller U, Feurer T. Ptychographic reconstruction of attosecond pulses. *Opt Express*. 2015;23(23):29502–29513.
28. Lucchini M, Nisoli M. Refined ptychographic reconstruction of attosecond pulses. *Appl Sci*. 2018;8(12):Article 2563.
29. Dolso GL, Inzani G, Di Palo N, Moio B, Medeghini F, Borrego-Varillas R, Nisoli M, Lucchini M, et al. Versatile and robust reconstruction of extreme-ultraviolet pulses down to the attosecond regime. *APL Photonics*. 2023;8(7):Article 076101.
30. Keathley P, Bhardwaj S, Moses J, Laurent G, Kärtner F. Volkov transform generalized projection algorithm for attosecond pulse characterization. *New J Phys*. 2016;18(7):Article 073009.
31. Orfanos I, Makos I, Liontos I, Skantzakis E, Förg B, Charalambidis D, Tzallas P. Attosecond pulse metrology. *APL Photon*. 2019;4(8):Article 080901.
32. Mikaelsson S, Vogelsang J, Guo C, Sytcevich I, Viotti AL, Langer F, Cheng YC, Nandi S, Jin W, Olofsson A, et al. A high-repetition rate attosecond light source for time-resolved coincidence spectroscopy. *J Nanophotonics*. 2021;10(1):117–128.
33. Wittmann T, Horvath B, Helml W, Schätzel MG, Gu X, Cavalieri AL, Paulus GG, Kienberger R. Single-shot carrier–envelope phase measurement of few-cycle laser pulses. *Nat Phys*. 2009;5(5):357–362.
34. Hernández-García C, Pérez-Hernández JA, Ramos J, Conejero Jarque E, Roso L, Plaja L. High order harmonic propagation in gases within the discrete dipole approximation. *Phys Rev A*. 2010;82(3):Article 033432.
35. Yudin G, Ivanov M. Nonadiabatic tunnel ionization: Looking inside a laser cycle. *Phys Rev A*. 2001;64(1):Article 013409.
36. Keldysh L. Ionization in the field of a strong electromagnetic wave. *Sov Phys JETP*. 1965;20(5):1307.
37. Perelomov A, Popov V, Terentev M. Ionization of atoms in an alternating electric field. *Sov Phys JETP*. 1966;5(23):1393–1409.
38. Constant E, Garzella D, Breger P, Mével E, Dorrer C, Le Blanc C, Salin F, Agostini P. Optimizing high harmonic generation in absorbing gases: Model and experiment. *Phys Rev Lett*. 1999;8(82):1668–1671.
39. Ruchon T, Hauri CP, Varjú K, Mansten E, Swoboda M, López-Martens R, L'Huillier A. Macroscopic effects in attosecond pulse generation. *New J Phys*. 2008;10(2):Article 025027.
40. Samson J, Stolte W. Precision measurements of the total photoionization cross-sections of He, Ne, Ar, Kr, and Xe. *J Electron Spectrosc Related Phenom*. 2002;123(2–3):265–276.
41. Murari M, Lucarelli G, Lucchini M, Nisoli M. Robustness of the ePIE algorithm for the complete characterization of femtosecond, extreme ultra-violet pulses. *Opt Express*. 2020;28(7):10210–10224.

Ultrafast Science
A SCIENCE PARTNER JOURNAL

Subcycle Phase Matching Effects in Short Attosecond Pulse Trains

Nedjma Ouahioune, Rodrigo Martin-Hernández, Dominik Hoff, Praveen Kumar Maroju, Chen Guo, Robin Weissenbilder, Sara Mikaelsson, Anne L'Huillier, Matteo Lucchini, Cord L. Arnold, and Mathieu Gisselbrecht

Citation: Ouahioune N, Martin-Hernández R, Hoff D, Maroju P, Guo C, Weissenbilder R, Mikaelsson S, L'Huillier A, Lucchini M, Arnold C, et al. Subcycle Phase Matching Effects in Short Attosecond Pulse Trains. *Ultrafast Sci*. 2026;**6**:0154. DOI: 10.34133/ultrafastscience.0154

Attosecond pulses produced by high-order harmonic generation in gases driven by intense laser fields have become a cornerstone technique for probing ultrafast electronic motion in matter. These applications require a good knowledge of the temporal and spectral properties of the emitted radiation. In this work, we generate a train of 2 to 3 attosecond pulses that we characterize using 2-color laser-assisted photoionization. An unexpected spectral behavior, with more pulses at high energies than at low energies, is observed when the carrier-to-envelope phase of the laser field is changed by 90°. High-order harmonic generation simulations indicate that the time-dependent phase matching of the harmonics contributes in a nontrivial way to the structure of the pulse train. Two-color laser-assisted photoionization enables us to unravel the dynamical influence of subcycle phase matching on the spectral properties of the attosecond pulse train, going beyond the predictions of the response of a single atom to a strong laser field.
Image

Ultrafast Science (ISSN 2765-8791) is published by the American Association for the Advancement of Science. 1200 New York Avenue NW, Washington, DC 20005.